European Journal of Radiology 150 (2022) 110259

Contents lists available at ScienceDirect

European Journal of Radiology

journal homepage: www.elsevier.com/locate/ejrad

Automated lung vessel segmentation reveals blood vessel volume redistribution in viral pneumonia

Julien Poletti [a,*], Michael Bach [b], Shan Yang [b], Raphael Sexauer [a], Bram Stieltjes [b], David C. Rotzinger [c], Jens Bremerich [a], Alexander Walter Sauter [a,b,1], Thomas Weikert [a,b,1]

[a] Department of Radiology, University Hospital Basel, University of Basel, Petersgraben 4, 4031 Basel, Switzerland
[b] Department of Research and Analysis, University Hospital Basel, University of Basel, Petersgraben 4, 4031 Basel, Switzerland
[c] Cardiothoracic and Vascular Division, Department of Diagnostic and Interventional Radiology, Lausanne University Hospital and University of Lausanne, Rue du Bugnon 46, 1011 Lausanne, Switzerland

ARTICLE INFO

Keywords:
Algorithms
Blood vessels
Viral pneumonia
COVID-19
Influenza

ABSTRACT

Purpose: It is known from histology studies that lung vessels are affected in viral pneumonia. However, their diagnostic potential as a chest CT imaging parameter has only rarely been exploited. The purpose of this study is to develop a robust method for automated lung vessel segmentation and morphology analysis and apply it to a large chest CT dataset.

Methods: In total, 509 non-enhanced chest CTs (NECTs) and 563 CT pulmonary angiograms (CTPAs) were included. Sub-groups were patients with healthy lungs (group_NORM, n = 634) and those RT-PCR-positive for Influenza A/B (group_INF, n = 159) and SARS-CoV-2 (group_COV, n = 279). A lung vessel segmentation algorithm (LVSA) based on traditional image processing was developed, validated with a point-of-interest approach, and applied to a large clinical dataset. Total blood vessel volume in lung (TBV) and the blood vessel volume percentage (BV%) of three blood vessel size types were calculated and compared between groups: small (BV5%, cross-sectional area < 5 mm^2), medium (BV5-10%, 5–10 mm^2) and large (BV10%, >10 mm^2).

Results: Sensitivity of the LVSA was 84.6% (95 %CI: 73.9–95.3) for NECTs and 92.8% (95 %CI: 90.8–94.7) for CTPAs. In viral pneumonia, besides an increased TBV, the main finding was a significantly decreased BV5% in group_COV (n = 14%) and group_INF (n = 15%) compared to group_NORM (n = 18%) [$p < 0.001$]. At the same time, BV10% was increased (group_COV n = 15% and group_INF n = 14% vs. group_NORM n = 11%; $p < 0.001$).

Conclusion: In COVID-19 and Influenza, the blood vessel volume is redistributed from small to large vessels in the lung. Automated LSVA allows researchers and clinicians to derive imaging parameters for large amounts of CTs. This can enhance the understanding of vascular changes, particularly in infectious lung diseases.

Abbreviations: BV, Blood Vessel Volume (ml); BV5, Blood Vessel Volume of vessels with cross-sectional area <5 mm^2; BV5-10, Blood Vessel Volume of vessels with cross-sectional area between 5 and 10 mm^2; BV10, Blood Vessel Volume of vessels with cross-sectional area >10 mm^2; BV%, Blood Vessel Volume percentage (%) (= the ratio BV/TBV); BV5%, Ratio BV5/TBV, which is the Blood Vessel Volume percentage of vessels with a cross-sectional area <5 mm^2; BV5-10%, Ratio BV5-10/TBV, which is the Blood Vessel Volume percentage of vessels with a cross-sectional area between 5 and 10 mm^2; BV10%, Ratio BV5-10/TBV, which is the Blood Vessel Volume percentage of vessels with a cross-sectional area > 10 mm^2; COPD, Chronic Obstructive Pulmonary Disease; COVID-19, Coronavirus Disease 2019; CT, Computed Tomography; CTPA, Computed Tomography Pulmonary Angiogram; HU, Hounsfield Unit; LVSA, Lung Vessel Segmentation Algorithm; NECT, Non-Enhanced Computed Tomography; PACS, Picture Archiving and Communication System; PGY, Postgraduate Year; POI, Point of Interest; RT-PCR, Reverse Transcription Polymerase Chain Reaction; SARS-CoV-2, Severe Acute Respiratory Syndrome Coronavirus 2; TBV, Total Blood Vessel Volume in Lung; TLV, Total Lung Volume; WHO, World Health Organization.

* Corresponding author at: Department of Radiology, University Hospital Basel, University of Basel, Petersgraben 4, 4031 Basel, Switzerland.
E-mail addresses: julien.poletti@unibas.ch (J. Poletti), michael.bach@usb.ch (M. Bach), shan.yang@usb.ch (S. Yang), raphael.sexauer@usb.ch (R. Sexauer), bram.stieltjes@usb.ch (B. Stieltjes), david.rotzinger@chuv.ch (D.C. Rotzinger), jens.bremerich@usb.ch (J. Bremerich), alexander.sauter@usb.ch (A. Walter Sauter), thomas.weikert@usb.ch (T. Weikert).
[1] Shared senior authors.

https://doi.org/10.1016/j.ejrad.2022.110259
Received 17 September 2021; Received in revised form 18 February 2022; Accepted 10 March 2022
Available online 17 March 2022

1. Introduction

Computed tomography (CT) is an important diagnostic tool for viral pneumonia, e.g. in COVID-19 patients. Beyond qualitative description of findings on CT, algorithms can be used to derive quantitative parameters important for the improvement of patient care [1]. Regarding pneumonia, algorithms targeting CT imaging features of lung parenchyma involvement, such as ground glass opacities and consolidations, have been extensively studied [2-5].

In contrast, only few imaging studies have explored the role of the pulmonary vasculature in viral pneumonia. From the few studies focusing on algorithm development for segmentation of pulmonary vasculature in COVID-19, it appears that the blood vessel volume is redistributed from smaller to larger vessels [6]. Moreover, blood vessel volume redistribution was used as an image parameter to predict clinical outcome [7]. This phenomenon has only rarely been addressed in radiology, despite full coverage of lung vessels in every chest CT scan and growing evidence for vascular involvement in COVID-19 from other fields of research: among others, microcirculation disturbances [8], coagulation activation [9], and hypoxic pulmonary vasoconstriction [10] were observed.

This leads us to the hypothesis that vascular imaging features may play an important role in viral pneumonia diagnosis. To further explore this hypothesis, methods for automated and batch-wise lung vessel analysis are required.

The three main goals of this study are therefore: (1) To develop and test an algorithm for automated segmentation of lung vessels. (2) To apply this algorithm to a large chest CT dataset of patients with COVID-19, Influenza, and controls (patients with healthy lungs). (3) To derive vascular imaging parameters and assess differences between the three patient groups.

2. Methods

This retrospective, single-center study has been conducted in line with the regulations of the local ethics committee (Ethikkommission Nordwest und Zentralschweiz, project IDs: Req-2020–00595 and 2020–00566).

2.1. Patient population

Three patient groups (SARS-CoV-2, Influenza A/B and control group) were compiled as follows:

2.2. Group_COV (SARS-CoV-2) and Group_INF (Influenza A/B)

All patients with a RT-PCR test positive for SARS-CoV-2 [between February 2020 and November 2020 (n = 3443)] and Influenza A or B [January 2014 - July 2020 (n = 3544)] were identified using the laboratory information system of our institution. The laboratory information system was checked to ensure that none of the patients was simultaneously positive for both COVID-19 and Influenza.

2.3. Group_NORM (control group)

Using an in-house Picture Archiving and Communication System (PACS) search tool (https://pacs-ris-crawler.github.io/), we identified all chest CT scans (NECT and CTPA) with unremarkable lungs acquired between January 2014 and July 2020. Inclusion criterion was a written radiology report describing an unremarkable lung parenchyma and central airways [search terms: “No focus of thoracic infection” AND “Open central airways” AND “No pleural effusion” AND “No pneumothorax” AND “No breathing artifacts”; reports at our institution are structured]. Finally, all reports were additionally reviewed by a radiology resident in the first postgraduate year (J.P.) to confirm the categorization. Subsequently, the laboratory information system was checked to ensure that none of the patients was positive for COVID-19 or Influenza. Fig. 1a and 1b provide a detailed study cohort flowchart.

2.4. Inclusion and exclusion criteria

In group_COV and group_INF, all NECTs and CTPAs performed ten days before or after the positive RT-PCR test were identified in the PACS. The rationale behind the period of ten days is that the disease and associated chest CT findings mainly evolve within this time [11].

For all groups, studies with description of motion artifacts or severe lung abnormalities [malignancy, lobectomy, atelectasis, and pneumothorax] in the written radiology report were excluded.

2.5. Clinical information

For all patients, information on comorbidities was extracted from the clinical data system. Information on comorbidities was missing for 61 patients (5.6%). Furthermore, to quantify each patient’s health state, a disease severity score (from 1 to 6) has been calculated according to a modified World Health Organization disease severity scale (WHO score) [12]. This scale is based on the patient’s oxygen demand and ventilation (Appendix A provides details).

2.6. CT acquisition parameters

CTs were acquired in supine position and full inspiration using four CT scanners (SOMATOM Definition Edge [128 slices] (n = 167), SOMATOM Definition AS + [128 slices] (n = 671), SOMATOM Definition Flash [2x128 slices] (n = 171), SOMATOM Force [2x192 slices] (n = 63). All scanners from Siemens Healthineers, Erlangen, Germany.

Acquisition parameters were as follows: mean peak tube voltage 103.0 kVp (SD: 12.9), mean tube current time product 140.4 mAs (SD: 94.0), mean computed tomography dose index (CTDI) 3.7 mGy (SD: 2.0), mean dose length product (DLP) 127.0 mGy*cm (SD: 68.7) and mean pitch 1.6 (SD: 0.6). Concerning CTPAs, Ultravist 370 (n = 514; Bayer HealthCare, Leverkusen, Germany), Iopamiro 370 (n = 46; Bracco Imaging, Milano, Italy) and Xenetix 350 (n = 3; Guebert, Villepinte, France) were used as contrast agents. The mean contrast media volume was 65.0 ml (SD: 12.3) and the mean flow rate 3.9 ml/s (SD: 0.3).

2.7. Lung segmentation and opacity quantification

The software NORA (http://www.nora-imaging.com) was used to organize, visualize, and annotate data. The lung masks were predicted by an established lung segmentation algorithm based on a Retina-U-Net (DICE score: 0.97) [13]. Knowing that lung vessels become narrower towards the periphery and to assess an influence of vessel diameter on segmentation accuracy, the lung segmentation mask was divided into three isovolumetric zones: central, middle, and peripheral (Fig. 2). The zones were defined both in the left and the right lung separately, which resulted in 6 lung zones per CT.

Furthermore, lung opacities (ground glass opacities and consolidations) were quantified using an established threshold of −600 to 0 Hounsfield units (HU) [5]. Relative high attenuation area between −600 and 0 HU (rHAA-600/0) is the ratio of opacity over total lung volume (TLV) and is expressed as a percentage.

2.8. Lung vessel segmentation

A fully automated lung vessel segmentation algorithm (LVSA) newly developed for this project and based on classical image processing algorithms was implemented in Python [14-18]. The vessel segmentation steps were limited to the area defined by the lung mask resulting from the previous segmentation step. In short, the contrast of the original dataset is increased by a filter. Local intensity maxima potentially correspond to voxels representing blood vessels. Considering other

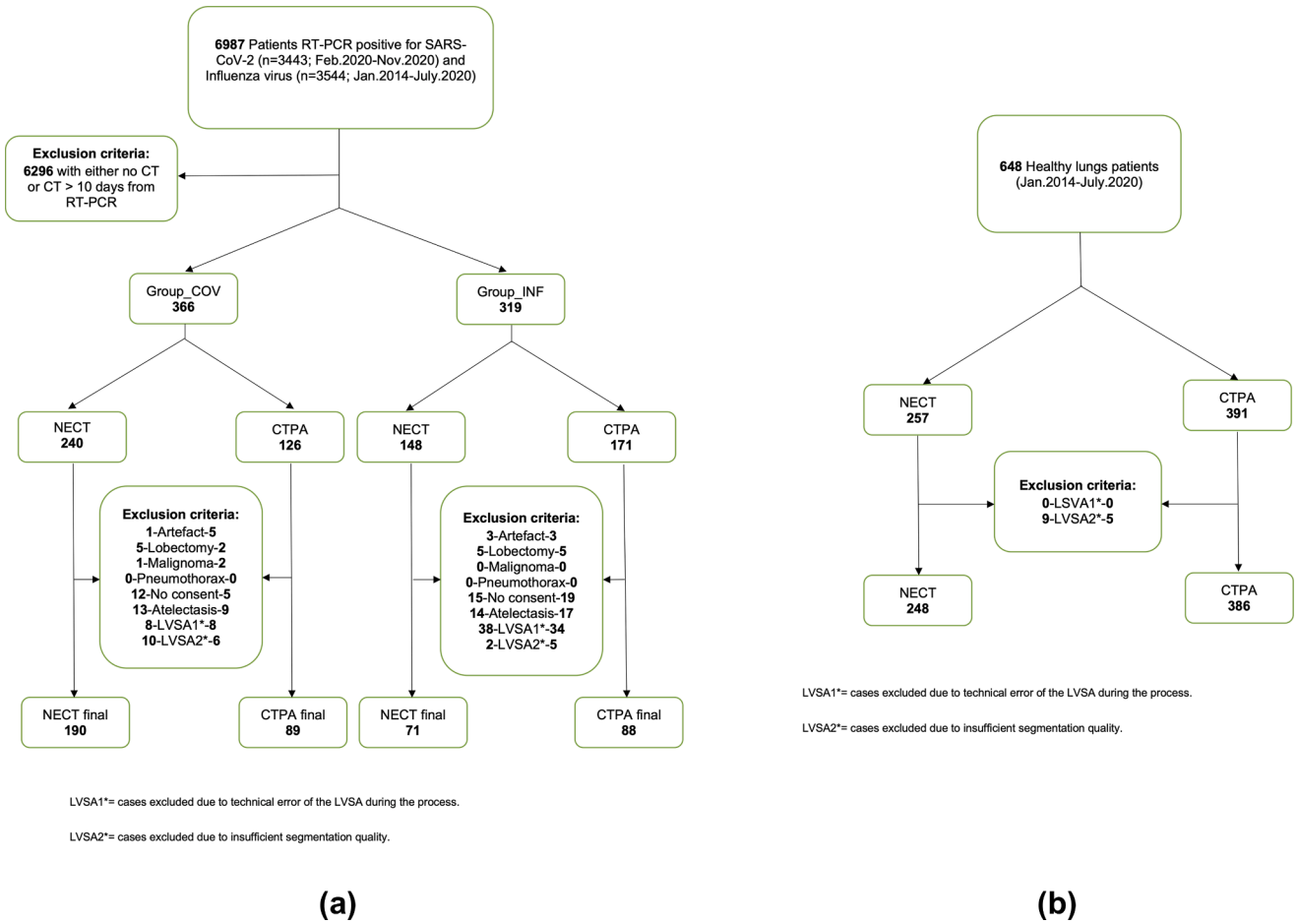

Fig. 1. Study selection flow chart (a) for group_COV and group_INF and (b) for group_NORM.

properties such as morphology (tube-like structure) and size of connected regions, the voxels most likely to correspond to blood vessels are identified. Via region growing, the result is the complete segmentation of the lung vessel tree, consisting of the vessel walls and the blood volume contained in the vessels (Fig. 3).

2.9. Internal and external LVSA validation

Internal LVSA validation was performed on 20 CTs, 10 NECTs and 10 CTPAs. The 20 exams were randomly selected to represent the complete pulmonary opacity spectrum (rHAA-600/0 range: 3.2%-70.0%; mean [NECT] = 23.8%; mean[CTPA] = 20.1%). To test LVSA performance, we adopted a method proposed by the VESSEL12 challenge [19]: A total of 160 points-of-interest (POIs) per lung were defined to mark two target structures: lung vessels (n = 60) and pulmonary parenchyma (n = 100). Regarding lung vessels, POIs were defined as follows: First, to avoid selection bias, 10 vessel POIs (arteries and veins) were randomly distributed in each zone. Then, radiology residents (J.P., PGY-1, R.S., PGY-4 and T.W., PGY-5) moved each POI to the artery/vein closest to the initial POI in axial orientation. In a second step, all POIs were individually checked by a board-certified radiologist with 11 years of experience in cardiothoracic imaging (A.W.S.) and modified, if needed.

The 100 pulmonary parenchymal POIs per scan were also randomly distributed and moved only if they were initially placed over a vessel or another non-parenchymal structure. The number of vessel and parenchymal POIs was equally distributed over the 6 lung zones. The proportion of POIs included in the vessel segmentation masks was calculated in total as well as for each scan and each region separately.

External validation was performed with 10 studies (5 NECT, 5 CTPA) from two independent datasets. The five CTPAs datasets are part of the COVID-CAVA study [20] and the five NECTs were provided by a regional hospital. POI analysis was conducted using the same methodology as during internal validation.

In addition, lung vessel segmentation quality of all cases was visually assessed by a supervised medical doctor (J.P.). If the segmentation quality of a case was rated unsatisfactory, it was discussed with a board-certified radiologist (A.W.S.) and potentially excluded in consensus (details and exemplary images in result section).

2.10. Lung vessel analysis

Starting points were the LVSA segmentation masks. Assuming a cylindrical vessel shape, the cross-sectional area corresponds to a specific number of voxels in each vessel segment. Each vessel voxel was assigned to one of the vessel size categories by counting the number of voxels in its neighborhood.

Thereby, the following imaging parameters were derived: First, the total blood vessel volume in lung (TBV) defined as the blood vessel volume of the vessel tree in ml. Second, the blood vessel volumes (BV) contained in three blood vessel types: vessels with a cross-sectional area $< 5\ mm^2$ (BV5), between 5 and 10 mm^2 (BV5-10) and $> 10\ mm^2$ (BV10). Third, the ratio of BV over TBV, labelled as blood vessel volume percentage (BV%), for each blood vessel type (BV5%, BV5-10% and BV10%). Each parameter has been calculated for the entire lung as well as for each lung zone separately.

A sub-analysis including those patients positive for SARS-CoV-2 and Influenza with rHAA-600/0 values equal to group_NORM was performed.

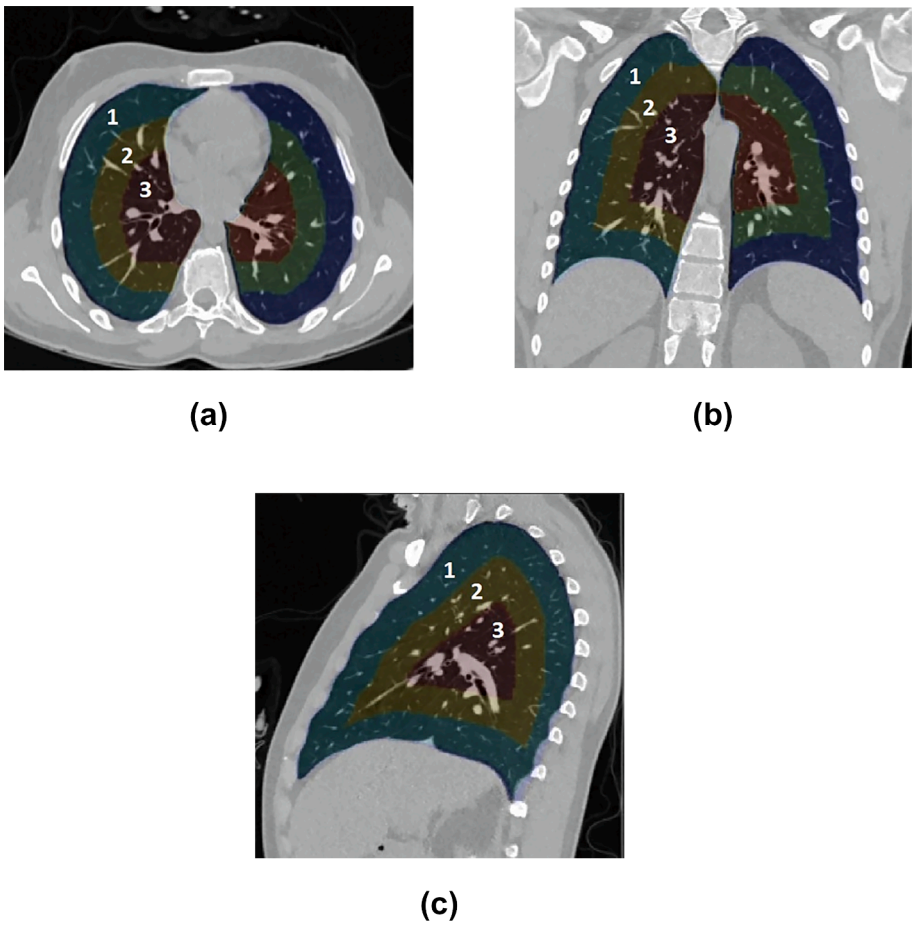

Fig. 2. Lung sub-division in three different zones signified as color overlay in a NECT of a 19-year-old female patient [group_NORM] in (a) axial, (b) coronal and (c) sagittal orientation. Number 1 labels the peripheral zone, number 2 the middle zone and number 3 the central zone.

2.11. Statistical analysis

Statistical analysis was performed using SPSS version 25.0 (SPSS Inc., Chicago, IL). P-values of ≤ 0.05 were considered statistically significant. To analyze group differences of continuous, normally distributed variables, T-Test [two groups] and one-way analysis-of-variance (ANOVA with Tukey-post-hoc test; three or more groups) were used. For comparison of categorical variables, Chi-square test was used. As part of an explorative analysis, the relationship between multiple patients' characteristics (age, sex, TLV, comorbidities, rHAA-600/0, and WHO score) and the BV%-imaging parameters were investigated using non-parametric Spearman rank correlation analysis. The correlation coefficients were classified as weak (0.010–0.290), moderate (0.300–0.390), strong (0.400–0.690) and very strong (>0.700). Due to collinearity between many of the variables we deliberately refrained from a regression model analysis. To assess normal distribution, Shapiro-Wilk test, histograms, and Q-Q plots were used.

3. Results

3.1. Study cohort characteristics

Of 1333 initially identified studies, 136 were excluded following the exclusion criteria. LVSA processing failed in 88 cases and 37 cases were excluded due to unsatisfactory vessel segmentation (Fig. 4). Pulmonary embolism was present in seven CTPAs for which the LVSA quality control did not find any vessel segmentation errors. A total of 1072 studies were included in the final analysis: n = 279 in group_COV (n = 190 NECT; n = 89 CTPA), n = 159 in group_INF (n = 71 NECT; n = 88 CTPA) and n = 634 in group_NORM (n = 248 NECT; n = 386 CTPA) (details: Fig. 1a and 1b).

Overall, viral infected patients were older ($p \leq 0.001$) and more likely to suffer from comorbidities such as hypertension ($p \leq 0.001$) (see Table 1). Group_COV showed an increased obesity rate (14.7%) when compared to group_INF (5.7%; $p = 0.007$) and group_NORM (5.4%; $p \leq 0.001$). The rHAA-600/0 rates ($p \leq 0.001$) and the WHO scores ($p \leq 0.001$) were higher in viral infected patients and TLV was significantly decreased (4245.0 ml; $p \leq 0.001$) in group_COV when compared to group_NORM (4638.9 ml).

3.2. Lung vessel segmentation algorithm evaluation

3.2.1. Internal validation

The overall sensitivity of the LVSA was 88.7% (95 %CI: 83.4–94.0), meaning 88.7% of POIs were included in the lung vessel segmentation mask. Of note, the performance was significantly better in CTPAs [92.8% (95 %CI: 90.8–94.7)] compared to NECTs [84.6% (95 %CI: 73.9–95.3)] ($p = 0.008$). A similar observation was made for the parenchymal POIs, in which 99.9% (95 %CI: 99.6–100; CTPA) and 97.4% (95 %CI: 94.4–100; NECT) did (correctly) not intersect with lung vessel segmentation mask ($p = 0.053$). The LVSA performance was significantly worse in the central zone compared to middle and peripheral zones (all: $p \leq 0.05$) (Table 2).

In the 20 patients used for internal validation, the mean rHAA-600/0 was 20.1% in CTPA and 23.6% in NECT. Correlation between the LVSA performance and the rHAA-600/0 rate in CTPAs (Rs = -0.333; p =

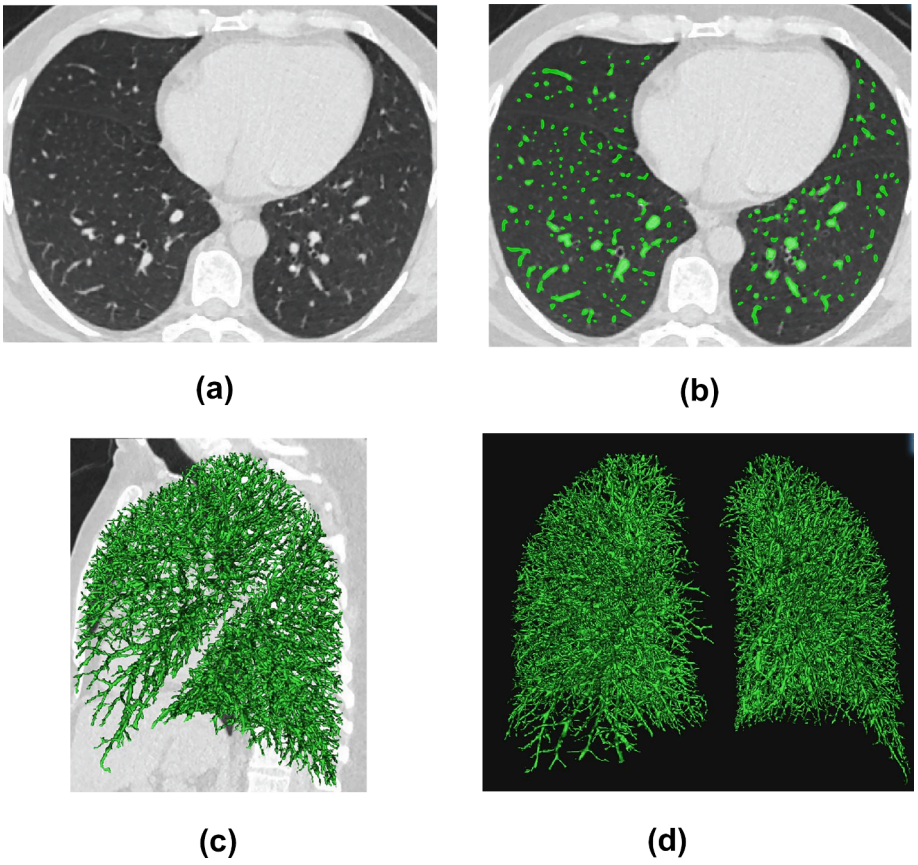

Fig. 3. Illustration of LVSA results on a CTPA scan of a 19-year-old patient from group_NORM: (a) Original CT scan in axial orientation, (b) CT scan with the lung vessel segmentation mask produced by the LVSA as green overlay. (c) and (d) are 3D representations of the lung vessel segmentation.

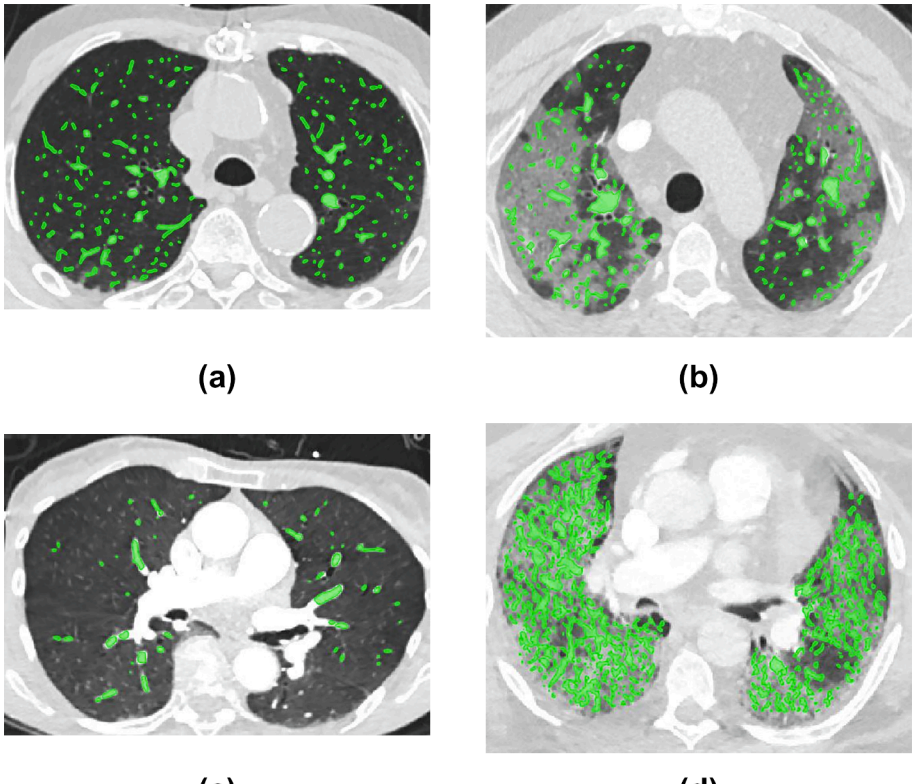

Fig. 4. Images illustrating the LVSA' s performance: (a) NECT from group_COV and (b) CTPA from group_COV showing two typical cases of successful lung vessel segmentation. Of note, even in case (b) with substantial areas of high opacity, the algorithm performance is good. (c) CTPA of a patient from group_NORM with relevant parts of the central lung vessels not segmented. (d) CTPA of a COVID-19 patient from group_COV showing a case of significant vessel oversegmentation due to pulmonary opacities.

Table 1
Patient characteristics including comorbidities.

	Entire cohort (NECT and CTPA)			NECT			CTPA		
Group	COV	INF	NORM	COV	INF	NORM	COV	INF	NORM
Total	279	159	634	190	71	248	89	88	386
Mean Age	59.8	63.3	50.6[a]	59.6	60.4	50.1[a]	60.4	65.6	50.9[a]
(SD)	(17.1)	(16.6)	(18.6)	(17.6)	(15.8)	(16.8)	(15.9)	(16.9)	(19.7)
Female	97	70	360	67	23	105	30[b]	47[b]	255[b]
(%)	(34.8)	(44.0)	(56.8)	(35.2)	(32.3)	(42.3)	(33.7)	(53.4)	(66)
Male	182	89	274	123	48	143	59[b]	41[b]	131[b]
(%)	(65.2)	(56.0)	(43.2)	(64.7)	(67.6)	(57.6)	(66.2)	(46.5)	(33.9)
Mean TLV in ml	4245.0[b]	4481.7	4638.9[b]	4400.7[b]	4781.9	5075.1[b]	3912.5[b]	4239.4	4358.8[b]
(SD)	(1309.7)	(1381.6)	(1255.7)	(1345.2)	(1513.10)	(1244.9)	(1169.5)	(1221.4)	(1181.9)
Mean rHAA-600/0	17.3[b]	11.8[b]	7.42[b]	14.9[b]	10.0[b]	5.4[b]	22.8[b]	13.3[b]	8.7[b]
(SD)	(12.2)	(8.0)	(3.9)	(10.7)	(6.8)	(1.5)	(13.4)	(8.6)	(4.4)
Mean WHO score	2.9[b]	2.6[b]	2.0[b]	2.9[b]	2.5[b]	2.1[b]	3.0	2.7	2.0[a]
(SD)	(1.3)	(1.2)	(0.5)	(1.3)	(1.1)	(0.4)	(1.2)	(1.2)	(0.5)
Comorbidities									
Asthma	25	11	35	20[b]	2	9[b]	5	9	26
(%)	(9.0)	(6.9)	(5.5)	(10.5)	(2.8)	(3.6)	(5.6)	(10.2)	(6.7)
COPD	6	22[a]	11	3[b]	6[b]	2	3[b]	16[b]	9[b]
(%)	(2.1)	(13.8)	(1.7)	(1.5)	(8.4)	(0.8)	(3.3)	(18.1)	(2.3)
Diabetes	62[b]	35	42[b]	43	13	14[a]	19	22	28[a]
(%)	(22.2)	(22.0)	(6.6)	(22.6)	(18.3)	(5.6)	(21.3)	(25)	(7.2)
Hypertension	122	63	132[a]	82	24	39[a]	40	39	93[a]
(%)	(43.7)	(39.6)	(20.8)	(42.7)	(33.8)	(15.7)	(44.9)	(44.3)	(24)
Cardiopathy*	57	40	84[a]	39	16	29[a]	18	24[b]	55[b]
(%)	(20.4)	(25.1)	(13.2)	(20.5)	(22.5)	(11.6)	(20.2)	(27.2)	(14.2)
Obesity	41[a]	9	34	30[a]	2	9	11	7	25
(%)	(14.7)	(5.7)	(5.4)	(15.7)	(2.8)	(3.6)	(12.3)	(7.9)	(6.4)

*"Cardiopathy" includes patients with history of coronary diseases, cardiac insufficiency, aortic stenosis, myocardial infarction, and heart surgery.
a = results is statistically significantly different from the two other groups. b = results is statistically significantly different from the other groups marked with b (P-value of ANOVA/Chi-square Test < 0.05). SD = standard deviation.

Table 2
LVSA evaluation results on the internal validation dataset.

	NECT	CTPA
Vessel POIs detected by the algorithm in the entire lung	508/600	557/600
(%, SD)	(84.6, 14.1)	(92.8, 2.5)
Peripheral zone	180/200	194/200
(%, SD)	(90.0, 10.7)	(97.0, 3.3)
Middle zone	178/200	197/200
(%, SD)	(89.0, 15.1)	(98.5, 2.2)
Central zone	150/200	166/200
(%, SD)	(75.0, 2.1)	(83.0, 7)
Parenchyma POIs not part of lung vessel mask in the entire lung	975/1000	999/1000
(%, SD)	(97.5, 3.9)	(99.9, 0.3)

POIs = points of interest. SD = standard deviation.

0.347) and NECTs (Rs = -0.620; p = 0.056) were not statistically significant.

3.2.2. External validation

The external validation showed LVSA sensitivity for CTPA of 91.9% (95 %CI: 88.9–95.0) and NECT of 92.9% (95 %CI: 91.2–94.7). The mean rHAA-600/0 of 8% in CTPA and 9% in NECT was statistically significantly lower compared to the internal validation dataset (in both cases: $p < 0.001$). As during internal validation, lower vessel detection rates were found in the central zone compared to middle and peripheral zones (CTPA: 88.0% [central], 96.0% [middle], and 92.0%[peripheral]; NECT: 90.0%, 93.0%, and 96.0%). However, differences between zones were not statistically significant (p-values ranging from $p = 0.235$ to $p = 0.646$).

3.3. Lung vessel imaging parameter analysis

3.3.1. Total blood vessel volume

For both NECTs and CTPAs, TBV of the whole lung was higher in group_COV (320.4 ml and 297.9 ml) and group_INF (312.7 ml and 279.4 ml) when compared to group_NORM (285.4 ml and 232.3 ml) with statistically significant differences ($p \leq 0.001$). However, an exception was noted between NECT group_INF and group_NORM, for which the difference was not statistically significant ($p = 0.108$) (details: Table 3 and Appendix B).

3.3.2. Blood vessel volume analysis according to different vessel sizes

Compared to group_NORM [BV5%: 18.4% (NECT) and 17.8% (CTPA)], BV5% was significantly lower in group_COV (NECT: 14.7%; CTPA: 14.0%) and group_INF (BV5%: 15.7% and 15.4%). On the contrary, BV10% was significantly higher in group_COV (15.1% and 16.5%) and group_INF (BV10%: 14.1% and 14.7%) compared to group_NORM (BV10%: 10.8% and 11.9%) (Fig. 5). This was true for all comparisons in the peripheral and middle zones ($p < 0.001$).

In the periphery, the BV5-10% between group_INF (NECT: 75.9%; CTPA: 74.6%) and group_NORM (75.5%; 74.5%) did not differ significantly. However, BV5-10% in group_COV (76.6%; 75.5%) was statistically significantly increased compared to group_NORM ($p \leq 0.001$).

Table 3
Imaging parameter results for group_COV, group_INF and group_NORM.

Group		COV			INF			NORM		
Entire Lung		**BV5**	**BV5-10**	**BV10**	**BV5**	**BV5-10**	**BV10**	**BV5**	**BV5-10**	**BV10**
BV%	**NECT**	14.7% [a]	70.2%	15.1% [a]	15.7% [a]	70.1%	14.2% [a]	18.4%	70.8%	10.8%
	CTPA	14.0% [b]	69.5% [a]	16.5% [b]	15.4% [b]	70.0%	14.7% [b]	17.8%	70.3%	11.9%
BV	**NECT**	46.3	224.5	49.5	48.8	219.3	44.6	52.1	202.4	30.9
(ml)	**CTPA**	41.9	206.6	50.3	41.5	195.3	42.6	41.2	163.1	28.0
TBV	**NECT**		320.4 [a]			312.7			285.4	
(ml)	**CTPA**		297.9 [a]			279.4 [a]			232.3	
Periphery		**BV5**	**BV5-10**	**BV10**	**BV5**	**BV5-10**	**BV10**	**BV5**	**BV5-10**	**BV10**
BV%	**NECT**	17.9% [a]	76.6% [a]	5.5% [a]	19.2% [a]	75.9%	4.9% [a]	22.7%	75.5%	1.8%
	CTPA	17.0% [b]	75.5% [a]	7.5% [b]	19.4% [b]	74.6%	6.0% [b]	23.2%	74.5%	2.2%
BV	**NECT**	25.6	115.3	9.4	26.2	106.6	7.4	27.7	94.7	2.4
(ml)	**CTPA**	23.6	109.8	11.5	23.4	97.6	9.0	22.2	74.4	2.5
TBV	**NECT**		150.3 [a]			140.2			124.9	
(ml)	**CTPA**		145.0 [a]			130.0 [a]			99.0	
Middle		**BV5**	**BV5-10**	**BV10**	**BV5**	**BV5-10**	**BV10**	**BV5**	**BV5-10**	**BV10**
BV%	**NECT**	12.1% [a]	67.0% [a]	20.9% [b]	13.1% [a]	68.6% [a]	18.3% [b]	15.5%	71.5%	13.1%
	CTPA	11.3% [b]	65.5 % [b]	23.5% [b]	12.5% [b]	68.3% [b]	19.2% [b]	14.7%	71.3%	14.0%
BV	**NECT**	14.7	82.3	27.0	15.8	82.5	22.0	16.4	75.7	14.1
(ml)	**CTPA**	12.9	75.4	27.9	13.2	74.3	22.4	13.1	62.9	12.9
TBV	**NECT**		124.0 [a]			120.3 [a]			106.2	
(ml)	**CTPA**		116.2 [a]			109.9 [a]			88.9	
Central		**BV5**	**BV5-10**	**BV10**	**BV5**	**BV5-10**	**BV10**	**BV5**	**BV5-10**	**BV10**
BV%	**NECT**	12.3% [a]	58.4%	29.3% [a]	12.7% [a]	57.9% [a]	29.4% [a]	14.7%	58.5%	26.7%
	CTPA	12.1% [a]	57.8%	30.0%	12.2% [a]	59.8% [b]	28.0%	13.1%	57.9%	29.0%
BV	**NECT**	5.6	26.0	13.0	6.7	30.1	15.2	7.9	31.7	14.3
(ml)	**CTPA**	4.0	19.4	10.4	4.7	23.4	11.2	5.6	24.7	12.5
TBV	**NECT**		44.6 [a]			52.0			53.9	
(ml)	**CTPA**		33.8 [a]			39.3			42.8	

Each vessel size category was compared to the same categories of the other groups (e.g. BV5%_COV vs. BV5%_INF vs. BV5%_NORM). Comparisons were made for BV% and TBV. The p-values are found in appendix B.
a = the difference in this metric compared to group_NORM is statistically significant ($p < 0.05$). b = the difference in this metric compared to the two other groups is statistically significant. Red numbers = the highest values in group_COV for BV% and TBV. Blue numbers = the lowest values in group_COV for BV% and TBV.

A sub-analysis focusing on viral infected patients (group_COV and group_INF) with relatively low parenchymatous involvement (within the rHAA-600/0 range of group_NORM), has shown the same features, namely a decreased BV5% while TBV and BV10% were increased. A slightly increased peripheral BV5-10% in group_COV was observed (Appendix C).

3.3.3. Correlation analyses

The correlation between age and BV%- imaging parameters was weak: BV5% ($R_s = -0.125$; $p \leq 0.001$), BV5-10% ($R_s = 0.094$; $p = 0.002$), and BV10% ($R_s = 0.021$; $p \leq 0.001$). The same was true concerning the sex and comorbidities (Table 4).

RHAA-600/0 and BV5% correlated strongly negatively ($R_s = -0.582$; $p \leq 0.001$), rHAA-600/0 and BV10% strongly positively ($R_s = 0.603$; $p \leq 0.001$) in the entire cohort. The strongest correlations were found in group_COV for both BV5% and BV10% ($R_s = -0.702$ and 0.718; $p \leq 0.001$). In both group_INF and group_NORM, moderate to weak correlations were found.

The WHO score was negatively correlated with BV5% ($R_s = -0.392$; $p \leq 0.001$) and positively correlated with BV10% ($R_s = 0.337$; $p \leq 0.001$) in the entire cohort. The strongest correlation between WHO score and BV5% was found in group_COV ($R_s = -0.452$; $p \leq 0.001$). Moreover, the strongest correlation between rHAA-600/0 and the WHO score was once again found in group_COV ($R_s = 0.548$; $p \leq 0.001$) (Table 4).

4. Discussion

This study confirms that the pulmonary vasculature is an important target structure for the development of imaging parameters in respiratory viral disease. It covered the development and application of a robust algorithm for lung vessel segmentation in chest CT which showed good segmentation performance. It revealed a decrease in blood vessel volume of small vessels (BV5%) and an increase in blood vessel volume of larger vessels (BV10%) as well as an increased TBV in patients with viral disease, reflecting blood vessel volume redistribution.

The lung is among the organs most affected by viral diseases such as Influenza A/B and SARS-CoV-2 [21]. There is rising evidence from histology studies that profound knowledge of pulmonary vascular pathophysiology is crucial to understand the complex processes in respiratory infectious diseases [22]. However, ex-vivo methods significantly alter lung physiology. Therefore, and because diagnostic methods for patients are required, there is demand for non-invasive imaging-based in-vivo methods [23].

Recently, Lins et al. [6] applied an automated blood vessel segmentation algorithm that performs an eigenvalue analysis of the Hessian matrix to enhance and identify tubular structures. Scans from COVID-19 patients (n = 103) showed a significant reduction of BV5% ($p \leq 0.001$) and significant increases of BV10%. This is in line with our observations. The absolute values differed between their study and ours (e.g. BV5 NORM: 30 ml vs. 18 ml; BV5 COVID-19: 25 ml vs. 14 ml, respectively). These differences could be caused by the differences in the algorithmic approaches. Nevertheless, the same basic observations were made, namely, a drastic decrease of BV5% and an increase of BV10% in COVID-19 compared to normal patients. The zone-specific approach (center, middle, periphery) adds more detail to the analysis: a significant drop of BV5% in all zones was shown for both COVID-19 and Influenza.

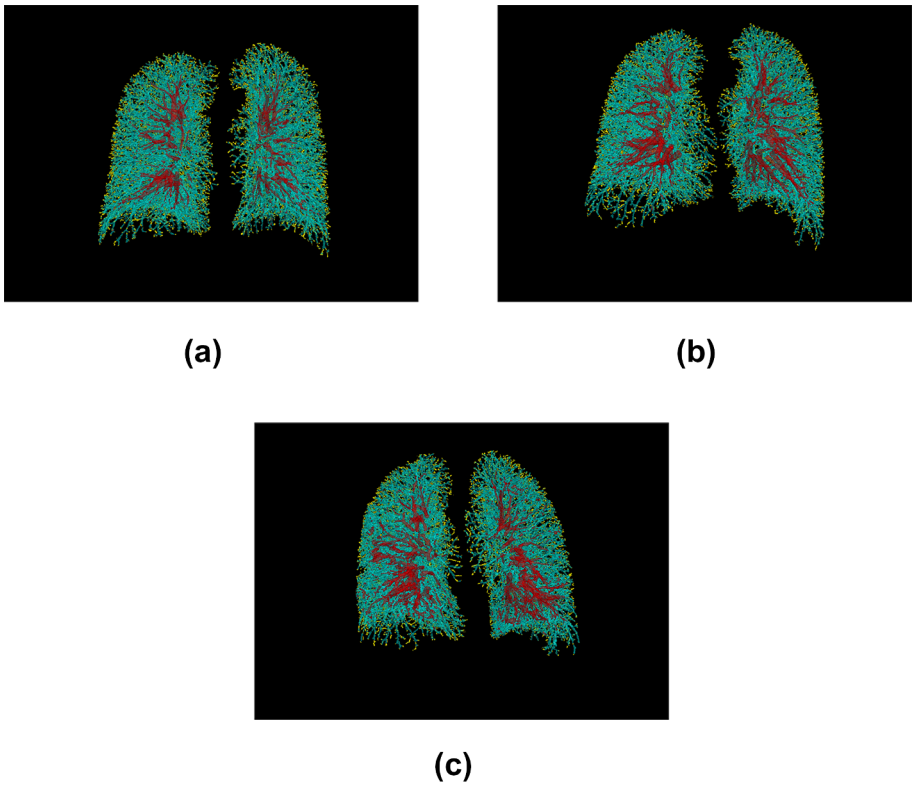

Fig. 5. 3D representation of the imaging parameter analysis illustrating the vessels distribution of BV5 (yellow), BV5-10 (blue) and BV10 (red) in: a) 60-year-old patient from group_NORM with typical blood vessel volume distribution. b) 50-year-old patient from group_INF with an increased portion of large vessels (red) spreading toward the pripheral part of the lung. (c) a 62-year-old patient from group_COV showing increased vascular diameter and volume distribution in the base of the lungs with a pronounced spread of larger vessels in the peripheral part when compared to (a) and (b).

In our study, the observed vascular changes were often more pronounced in COVID-19 than in Influenza. A possible explanation for this could be the difference in location of the viral receptor entry gates: the vascular endothelial cells in COVID-19 [24], the respiratory tract cells in influenza [25]. Variations in TBV and BV% were also observed in viral infected patients with rHAA-600/0 values comparable to group_NORM, suggesting that vascular involvement might be a distinct feature of viral infection.

As the frequencies of some comorbidities relevant to the size of lung vessels such as COPD and cardiopathy [26,27] differed significantly between the three patient groups, the observed vessel size changes are likely partly explained by this fact. However, the correlations with the BV%-imaging parameters were weak, pointing towards the fact that the vascular changes were mostly the consequence of viral infection. The same observations were made for age, sex and TLV.

We know from histology studies that the vascular alterations are related to inflammation and microcirculatory changes, which provide a likely explanation for the observed phenomenon [8]. BV%-imaging parameters and opacity have been described to be in close relationship in COVID-19 [28,29], a finding confirmed in this study: the opacity rate (rHAA-600/0) correlated positively with BV10% and negatively with BV5%. We also found a strong correlation between rHAA-600/0 and the WHO score [5]. Moreover, the strong negative correlation between the WHO score and BV5% in COVID-19 is in line with findings of Morris et al. [7], who suggested BV5% as a novel biomarker for predicting adverse outcomes in patients with COVID-19 seeking acute medical care. Therefore, a potential clinical use of the algorithm is the detection of early blood vessel changes to predict adverse clinical outcomes. To enable the swift exploration of other clinical use cases, the algorithm is implemented in a local clinic-near research platform accessible to radiologists and researchers of our department. Furthermore, the algorithm code is published on GitHub.

The POI vessel performance analysis revealed a good performance of our algorithm. Despite a slightly better LVSA performance in CTPAs compared to NECTs, the same changes of blood vessel volume distribution were observed in both groups. Regarding the high-level architecture, the algorithms that participated in the VESSEL12 challenge differed significantly from ours and from each other [19]. An objective comparison is hampered by the fact that most algorithms are not publicly available. We believe that in times of a global pandemic, fast scientific exchange is only possible with an open-source approach and therefore we have published our algorithm on GitHub (https://github.com/fsc-mib/travel).

On the internal validation dataset, the LVSA performed well in NECTs (84.6%), but even better in CTPAs (92.8%). This can be explained by the improved vessel-parenchyma contrast inherent to CTPAs. The external validation yielded a similar result for CTPAs (91.9%), but a markedly improved performance on NECTs (92.9%). Because the mean rHAA-600/0 was much lower in the external validation dataset compared to the internal validation dataset, this is plausible: The higher amount of parenchymal opacities in the internal dataset decreases the performance on NECTs, but not on CTPAs with their vascular contrast agent that has much higher HU-values than the opacities.

This study has limitations. First, the LVSA does not distinguish between arteries and veins. It is possible that vessel types are affected differently by viral infections. However, also the aforementioned studies did not make this discrimination, facilitating comparability. Second, the LVSA performance in the central zone was not as accurate as in the other two zones, a fact that is important when applying the algorithm. A possible reason would be that the maximum size of the blood vessels within the lung mask depends on the exact shape of this mask. The blood vessels being larger in the central zone, with size varying greatly from patient to patient, the algorithm might have problems in completely detecting these very large blood vessels. Third, while the negative correlation between rHAA-600/0 and vessel detection rate in NECTs was not statistically significant, it showed a strong statistical trend. Therefore, the opacity rate in NECTs could affect the LVSA performance. Fourth, LVSA processing failed in 6.6% of all cases. The main reason for algorithm failure in these cases was the presence of small artifacts in the image acquisition mainly caused by metal implants or external devices,

Table 4
Correlation between BV% and patient characteristics.

	BV5%	BV5-10%	BV10%
Age	R_s = -0.125; **p ≤ 0.001**	R_s = 0.094; **p = 0.002**	R_s = 0.021; p = 0.493
Sex	R_s = 0.198; **p ≤ 0.001**	R_s = 0.180; **p ≤ 0.001**	R_s = -0.266; **p ≤ 0.001**
TLV	R_s = 0.216; **p ≤ 0.001**	R_s = 0.001; p = 0.998	R_s = -0.180; **p ≤ 0.001**
Asthma	R_s = -0.016; p = 0.604	R_s = 0.053; p = 0.090	R_s = -0.007; p = 0.817
COPD	R_s = -0.080; **p = 0.011**	R_s = 0.030; p = 0.339	R_s = 0.051; p = 0.104
Diabetes	R_s = -0.239; **p ≤ 0.001**	R_s = -0.058; p = 0.063	R_s = 0.217; **p ≤ 0.001**
Hypertension	R_s = -0.211; **p ≤ 0.001**	R_s = 0.004; p = 0.898	R_s = 0.163; **p ≤ 0.001**
Cardiopathy	R_s = -0.139; **p ≤ 0.001**	R_s = 0.052; p = 0.100	R_s = 0.082; p = 0.082
Obesity	R_s = -0.219; **p ≤ 0.001**	R_s = 0.014; p = 0.647	R_s = 0.167; **p ≤ 0.001**
rHAA-600/0: entire cohort	R_s = -0.582; **p ≤ 0.001**	R_s = -0.219; **p ≤ 0.001**	R_s = 0.603; **p ≤ 0.001**
rHAA-600/0: group_COV	R_s = -0.702; **p ≤ 0.001**	R_s = -0.294; **p ≤ 0.001**	R_s = 0.718; **p ≤ 0.001**
rHAA-600/0: group_INF	R_s = -0.632; **p ≤ 0.001**	R_s = -0.251; **p ≤ 0.001**	R_s = 0.618; **p ≤ 0.001**
rHAA-600/0: group_NORM	R_s = -0.308; **p ≤ 0.001**	R_s = -0.140; **p ≤ 0.001**	R_s = 0.366; **p ≤ 0.001**
WHO: entire cohort	R_s = -0.392; **p ≤ 0.001**	R_s = -0.067; **p = 0.028**	R_s = 0.337; **p ≤ 0.001**
WHO: group_COV	R_s = -0.452; **p ≤ 0.001**	R_s = -0.079; p = 0.186	R_s = 0.396; **p ≤ 0.001**
WHO: group_INF	R_s = -0.356; **p ≤ 0.001**	R_s = -0.041; p = 0.608	R_s = 0.264; **p ≤ 0.001**
WHO: group_NORM	R_s = -0.005; p = 0.904	R_s = 0.029; p = 0.467	R_s = -0.003; p = 0.940

The exploratory analysis has been performed using the non-parametric Spearman Rank correlation analysis. Statistically significant p-values are in bold print. R_s = Spearman's rank correlation coefficient.

which resulted in artificial density changes in the lung parenchyma. This in turn significantly reduced the performance of the algorithm which for the moment limits its clinical applicability. A potential counterstrategy would be to use an AI-based vessel segmentation algorithm to increase robustness.

To conclude, this study developed, tested, and applied an automated method for a comprehensive assessment of lung vessels in NECT and CTPA. The most important findings are an increased TBV and an increased blood vessel volume of larger lung vessels (BV10) in patients RT-PCR positive for viral disease (COVID-19 and Influenza). This provides a quantitative confirmation of qualitative results from other fields of research. Automated lung vessel analysis is a valuable source of imaging parameters that deserves further investigation.

5. Data availability

The LVSA algorithm used is available on GitHub: https://github.com/fsc-mib/travel.

A sample dataset of 20 NECTs / CTPAs coming from the study cohort is freely available on: https://www.rapmed.net/#/publications/NECT-CTPA. Cases 1 to 10 belong to group_NORM; Cases 11, 12, 13 and 16 belong to group_INF; Cases 14, 15, 17, 18, 19 and 20 belong to group_COV.

CRediT authorship contribution statement

Julien Poletti: Conceptualization, Methodology, Software, Validation, Investigation, Data curation, Writing – original draft, Writing – review & editing, Visualization. **Michael Bach:** Methodology, Software, Validation, Formal analysis, Investigation, Data curation, Writing – original draft, Writing – review & editing, Visualization. **Shan Yang:** Methodology, Software, Validation, Investigation, Writing – original draft, Writing – review & editing, Visualization, Project administration. **Raphael Sexauer:** Validation, Investigation. **Bram Stieltjes:** Software, Formal analysis, Resources, Data curation, Writing – review & editing. **David C. Rotzinger:** Validation, Resources, Data curation, Writing – review & editing. **Jens Bremerich:** Conceptualization, Resources, Writing – review & editing, Project administration. **Alexander Walter Sauter:** Conceptualization, Methodology, Validation, Formal analysis, Investigation, Resources, Writing – review & editing, Supervision. **Thomas Weikert:** Conceptualization, Methodology, Software, Validation, Formal analysis, Investigation, Resources, Data curation, Writing – original draft, Writing – review & editing, Supervision, Project administration.

Acknowledgement

We appreciate the valuable contributions of the following employees of the University Hospital Basel: Dr. Christoph Aberle, PhD (radiology data retrieval), Dr. Fabian Franzeck, MD (clinical data retrieval), Dr. Carl Glessgen, MD (algorithm validation), Adrian Wilder-Smith, MD (professional English proofreading) and Dr. Jan Roth, MD, epidemiologist (statistical advice).

Appendix A. Supplementary data

Supplementary data to this article can be found online at https://doi.org/10.1016/j.ejrad.2022.110259.

References

[1] A.B. Rosenkrantz, M. Mendiratta-Lala, B.J. Bartholmai, D. Ganeshan, R. G. Abramson, K.R. Burton, J.-P. Yu, E.M. Scalzetti, T.E. Yankeelov, R. M. Subramaniam, L. Lenchik, Clinical utility of quantitative imaging, Academic Radiology 22 (1) (2015) 33–49.
[2] K. Li, J. Wu, F. Wu, D. Guo, L. Chen, Z. Fang, C. Li, The Clinical and Chest CT Features Associated With Severe and Critical COVID-19 Pneumonia, Investigative Radiology 55 (6) (2020) 327–331.
[3] H.Y.F. Wong, H.Y.S. Lam, A.-T. Fong, S.T. Leung, T.-Y. Chin, C.S.Y. Lo, M.-S. Lui, J. C.Y. Lee, K.-H. Chiu, T.-H. Chung, E.Y.P. Lee, E.Y.F. Wan, I.F.N. Hung, T.P.W. Lam, M.D. Kuo, M.-Y. Ng, Frequency and Distribution of Chest Radiographic Findings in Patients Positive for COVID-19, Radiology 296 (2) (2020) E72–E78.
[4] S. Altmayer, M. Zanon, G.S. Pacini, G. Watte, M.C. Barros, T.L. Mohammed, N. Verma, E. Marchiori, B. Hochhegger, Comparison of the computed tomography findings in COVID-19 and other viral pneumonia in immunocompetent adults: a systematic review and meta-analysis, European Radiology 30 (12) (2020) 6485–6496.
[5] A. Romanov, M. Bach, S. Yang, F.C. Franzeck, G. Sommer, C. Anastasopoulos, J. Bremerich, B. Stieltjes, T. Weikert, A.W. Sauter, Automated CT Lung Density Analysis of Viral Pneumonia and Healthy Lungs Using Deep Learning-Based Segmentation, Histograms and HU Thresholds, Diagnostics (Basel) 11 (5) (2021) 738, https://doi.org/10.3390/diagnostics11050738.
[6] M. Lins, J. Vandevenne, M. Thillai, B.R. Lavon, M. Lanclus, S. Bonte, R. Godon, I. Kendall, J. De Backer, W. De Backer, Assessment of Small Pulmonary Blood Vessels in COVID-19 Patients Using HRCT, Academic Radiology 27 (10) (2020) 1449–1455.
[7] M.F. Morris, Y. Pershad, P. Kang, L. Ridenour, B. Lavon, M. Lanclus, R. Godon, J. De Backer, M.K. Glassberg, Altered pulmonary blood volume distribution as a biomarker for predicting outcomes in COVID-19 disease, European Respiratory J. 58 (3) (2021) 2004133, https://doi.org/10.1183/13993003.04133-2020.
[8] M. Ackermann, S.E. Verleden, M. Kuehnel, A. Haverich, T. Welte, F. Laenger, A. Vanstapel, C. Werlein, H. Stark, A. Tzankov, W.W. Li, V.W. Li, S.J. Mentzer, D. Jonigk, Pulmonary Vascular Endothelialitis, Thrombosis, and Angiogenesis in Covid-19, New England J. Medicine 383 (2) (2020) 120–128.
[9] K. Mueller-Peltzer, T. Krauss, M. Benndorf, C.N. Lang, F. Bamberg, C. Bode, D. Duerschmied, D.L. Staudacher, V. Zotzmann, Pulmonary artery thrombi are co-located with opacifications in SARS-CoV2 induced ARDS, Respiratory Medicine 172 (2020), 106135.

[10] L. Gattinoni, S. Coppola, M. Cressoni, M. Busana, S. Rossi, D. Chiumello, COVID-19 Does Not Lead to a "Typical" Acute Respiratory Distress Syndrome, Am. J. Respiratory Critical Care Medicine 201 (10) (2020) 1299–1300.
[11] M. Francone, F. Iafrate, G.M. Masci, S. Coco, F. Cilia, L. Manganaro, V. Panebianco, C. Andreoli, M.C. Colaiacomo, M.A. Zingaropoli, M.R. Ciardi, C.M. Mastroianni, F. Pugliese, F. Alessandri, O. Turriziani, P. Ricci, C. Catalano, Chest CT score in COVID-19 patients: correlation with disease severity and short-term prognosis, European Radiology 30 (12) (2020) 6808–6817.
[12] W. Blueprint, novel coronavirus COVID-19 therapeutic trial synopsis, Switzerland, Geneva, 2020.
[13] C. Anastasopoulos, T. Weikert, S. Yang, A. Abdulkadir, L. Schmulling, C. Buhler, F. Paciolla, R. Sexauer, J. Cyriac, I. Nesic, R. Twerenbold, J. Bremerich, B. Stieltjes, A.W. Sauter, G. Sommer, Development and clinical implementation of tailored image analysis tools for COVID-19 in the midst of the pandemic: The synergetic effect of an open, clinically embedded software development platform and machine learning, European J. Radiology 131 (2020), 109233.
[14] R.G. Van, F. Drake, Python 3 reference manual, Scotts Valley, CreateSpace, CA, 2009.
[15] P. Virtanen, R. Gommers, T.E. Oliphant, M. Haberland, T. Reddy, D. Cournapeau, E. Burovski, P. Peterson, W. Weckesser, J. Bright, SciPy 1.0: fundamental algorithms for scientific computing in Python, Nature Methods 17 (3) (2020) 261–272.
[16] S. Van der Walt, J.L. Schönberger, J. Nunez-Iglesias, F. Boulogne, J.D. Warner, N. Yager, E. Gouillart, T. Yu, Scikit-image: image processing in Python, PeerJ 2 (2014), e453.
[17] V. Stimper, S. Bauer, R. Ernstorfer, B. Scholkopf, R.P. Xian, Multidimensional contrast limited adaptive histogram equalization, IEEE Access 7 (2019) 165437–165447.
[18] P.-S. Liao, T.-S. Chen, P.-C. Chung, A fast algorithm for multilevel thresholding, J. Inf. Sci. Eng. 17 (5) (2001) 713–727.
[19] R.D. Rudyanto, S. Kerkstra, E.M. van Rikxoort, C. Fetita, P.Y. Brillet, C. Lefevre, W. Xue, X. Zhu, J. Liang, I. Oksuz, D. Unay, K. Kadipasaoglu, R.S. Estepar, J. C. Ross, G.R. Washko, J.C. Prieto, M.H. Hoyos, M. Orkisz, H. Meine, M. Hullebrand, C. Stocker, F.L. Mir, V. Naranjo, E. Villanueva, M. Staring, C. Xiao, B.C. Stoel, A. Fabijanska, E. Smistad, A.C. Elster, F. Lindseth, A.H. Foruzan, R. Kiros, K. Popuri, D. Cobzas, D. Jimenez-Carretero, A. Santos, M.J. Ledesma-Carbayo, M. Helmberger, M. Urschler, M. Pienn, D.G. Bosboom, A. Campo, M. Prokop, P. A. de Jong, C. Ortiz-de-Solorzano, A. Munoz-Barrutia, B. van Ginneken, Comparing algorithms for automated vessel segmentation in computed tomography scans of the lung: the VESSEL12 study, Medical Image Analysis 18 (7) (2014) 1217–1232.
[20] S.D. Qanadli, A.W. Sauter, H. Alkadhi, A. Christe, P.-A. Poletti, L. Ebner, D. C. Rotzinger, Vascular Abnormalities Detected with Chest CT in COVID-19: Spectrum, Association with Parenchymal Lesions, Cardiac Changes, and Correlation with Clinical Severity (COVID-CAVA Study), Diagnostics 11 (4) (2021) 606.
[21] C.J. Burrell, C.R. Howard, F.A. Murphy, Fenner and White's Medical Virology, Elsevier, 2017, pp. 77–104.
[22] M.R. Chamarthy, A. Kandathil, S.P. Kalva, Pulmonary vascular pathophysiology, Cardiovasc. Diagn. Ther. 8 (3) (2018) 208–213.
[23] T. Sutherland, C. O'Donnell, The artefacts of death: CT post-mortem findings, J. Med. Imaging Radiat. Oncol. 62 (2) (2018) 203–210.
[24] Y.R. Guo, Q.D. Cao, Z.S. Hong, Y.Y. Tan, S.D. Chen, H.J. Jin, K.S. Tan, D.Y. Wang, Y. Yan, The origin, transmission and clinical therapies on coronavirus disease 2019 (COVID-19) outbreak - an update on the status, Military Medical Research 7 (1) (2020) 11.
[25] A. Garcia-Sastre, Influenza virus receptor specificity: disease and transmission, Am. J. Pathology 176 (4) (2010) 1584–1585.
[26] R. Malhotra, B.P. Dhakal, A.S. Eisman, P.P. Pappagianopoulos, A. Dress, R. B. Weiner, A.L. Baggish, M.J. Semigran, G.D. Lewis, Pulmonary vascular distensibility predicts pulmonary hypertension severity, exercise capacity, and survival in heart failure, Circulation, Heart Failure 9 (6) (2016), e003011.
[27] Y.H. Cho, S.M. Lee, J.B. Seo, N. Kim, J.P. Bae, J.S. Lee, Y.-M. Oh, S. Do-Lee, Quantitative assessment of pulmonary vascular alterations in chronic obstructive lung disease: associations with pulmonary function test and survival in the KOLD cohort, European J. Radiology 108 (2018) 276–282.
[28] H. Lv, T. Chen, Y. Pan, H. Wang, L. Chen, Y. Lu, Pulmonary vascular enlargement on thoracic CT for diagnosis and differential diagnosis of COVID-19: a systematic review and meta-analysis, Ann Transl Med 8(14) (2020) 878.
[29] Q. Li, X.-T. Huang, C.-H. Li, D. Liu, F.-J. Lv, CT features of coronavirus disease 2019 (COVID-19) with an emphasis on the vascular enlargement pattern, European J. Radiology 134 (2021), 109442.